Conceptual Design of an Optical Array Receiver, with Preliminary Experimental Results

V. Vilnrotter,[1] K. Andrews,[1] C. Lau,[1] and M. Srinivasan[1]

An attractive architecture for the ground receiving station of a deep-space optical communications link consists of an array of commercially available 76.2-cm telescopes and signal-combining electronics. This article describes such an array and presents results from proof-of-concept experiments using a commercial telescope, charge-coupled device (CCD) detector, and auto-guiding computer. These experiments show that while commercial telescopes are well suited to this application, significant work will be required in signal-processing algorithm design and implementation. The experiments also validate the mathematical models of atmospheric turbulence used in earlier analytical work and confirm the feasibility of a telescope array receiver.

I. Introduction

A stated objective of future deep-space missions is to dramatically increase the useful data rate, thus achieving greater science data return from each mission. This goal can be accomplished effectively through the use of optical rather than RF wavelengths. Due to cost and complexity considerations, the most practical approach at the present time is to employ a ground-based receiver, designed to mitigate the effects of atmospheric turbulence for best performance. A cost-effective approach for ground-based optical communications is the synthesis of a large optical aperture by means of an array of smaller telescopes.

In addition to the theoretical feasibility of array reception as shown in [1], array receivers offer additional advantages over single-aperture receivers for ground-based reception of optical signals, including graceful performance degradation in case of telescope failure, ease of future expansion to increase throughput or extend communications range, relaxed performance requirements on telescopes, and reduced implementation cost. The theoretical equivalence of the array receiver and the "single large telescope" receiver under operating conditions of interest has been shown in [1]. In this article, we present a conceptual design of the optical array, including a detailed description of an array element, identify its critical functional requirements, and describe the experimental evaluation of a candidate 63.5-cm optical telescope designed specifically for array applications.

---

[1] Communications Systems and Research Section.

The research described in this publication was carried out by the Jet Propulsion Laboratory, California Institute of Technology, under a contract with the National Aeronautics and Space Administration.

II. Conceptual Design of an Optical Array Receiver

A conceptual block diagram of the optical array receiver is shown in Fig. 1, which includes as part of the array a photograph of the 63.5-cm New Technology Telescope (NTT) manufactured by Jim's Mobile, Inc. (JMI) of Colorado. This telescope was selected and procured for evaluation on the basis of functional capabilities, rugged construction, excellent optics, and reasonable cost. Although only three elements are shown in Fig. 1, an operational array may contain a much larger number of telescopes, depending on the total collecting area required for a particular mission.

Control of the array is accomplished through the user interface, which also supplies critical information necessary for array operation to the telescopes. It is assumed that each telescope is equipped with a focal-plane array (FPA) capable of responding to single photon-detection events. Each telescope also has digital subsystems that are capable of deriving pointing corrections based on local measurements to update or fine-tune telescope pointing, optimize the FPA configuration in real-time to minimize the bit-error rate of the combined array output signal, and convert the FPA outputs into useful digital samples suitable for transmission to the central array combining assembly.

Following initial pointing acquisition, each telescope generates real-time pointing corrections computed from the signal distributions impinging on the focal-plane array of each telescope, estimates the extent of the turbulence-degraded point-spread function, and rapidly selects the detector elements containing the greatest signal energy in order to counter the effects of turbulence, as described in [2]. Telescope pointing can be conveniently accomplished in two steps: first, large accumulated pointing errors are fed back to the telescope drive assembly, repointing the entire instrument, and second, small excursions of the signal distribution from the center of the array are corrected via a fast-response tip–tilt mirror that responds to real-time pointing updates generated by the FPA electronics.

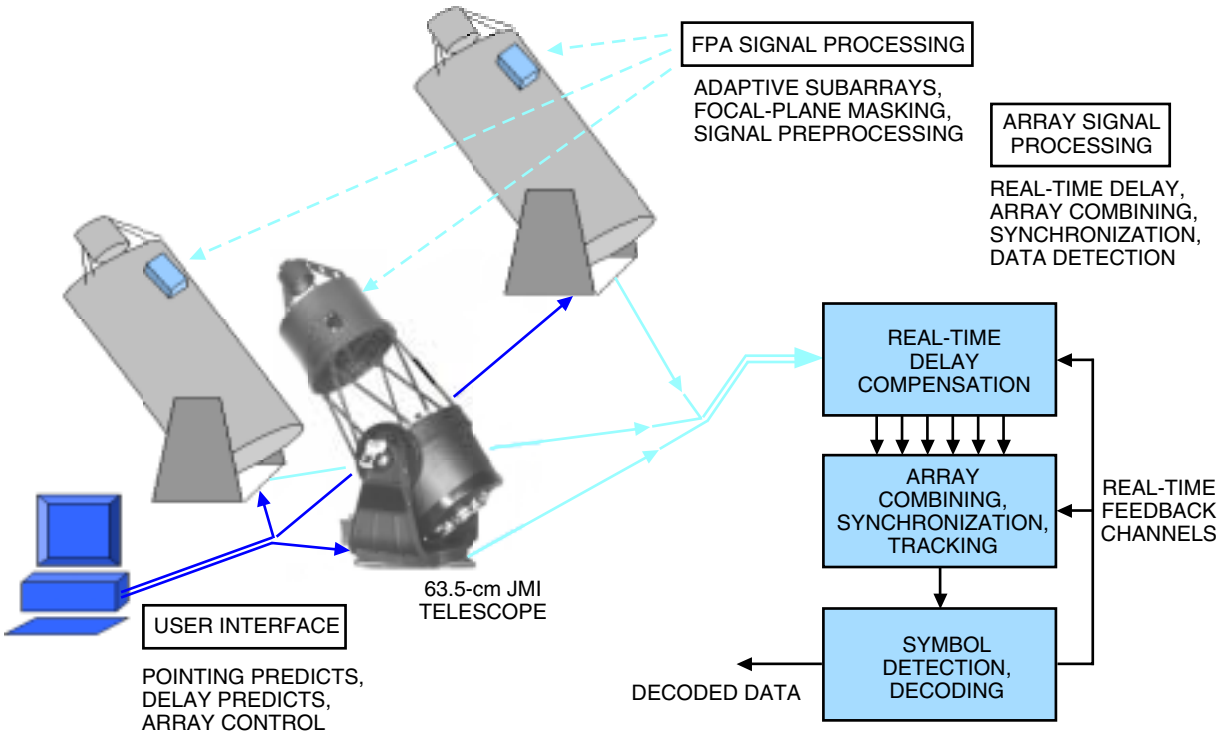

Fig. 1. Optical array receiver conceptual block diagram, including a photograph of the JMI 63.5-cm New Technology Telescope, as a representative element of the array.

The electrical signals generated at each telescope by the FPA signal processing assembly are transmitted through wideband cables or fiber-optic networks to a central array processing station, where further signal conditioning and processing necessary for data detection and decoding are carried out. First, the relative time delay between signals from different telescopes is measured and removed. Next, the delay-compensated signals are combined in the array combiner assembly to form a single sample stream with the goal of optimizing array performance. Finally, the combined samples are processed to effect slot synchronization, followed by symbol synchronization, frame synchronization, and continuously updated Doppler compensation (tracking). At this point, symbol detection can take place, or the fully synchronized and combined samples can be formatted and sent to the decoder along with other necessary parameter estimates and side information required by the decoder for decoding the transmitted information and distributing it to the end users of the data.

In order to carry out these operations, each telescope must be able to point to the commanded position in the sky, to an accuracy determined by the widest field-of-view (FOV) detector on the telescope, and then refine its pointing automatically to acquire and center the desired source within the much narrower FOV of the high-speed communications detector array located in the focal plane. Since there is significant scattered sunlight during the day everywhere in the sky, particularly when looking close to the Sun, a narrowband optical filter is essential to suppress unwanted background light. In addition, since background radiation is either unpolarized or only slightly polarized in certain specific directions relative to the Sun, a polarizing filter can be used to further suppress the polarization component orthogonal to the signal polarization. Implementing these operations requires optical and mechanical design specifically tailored to the components that carry out the desired functions.

The optical design shown in Fig. 2 is based on the 76.2-cm NTT also manufactured by JMI, Inc., and similar in design to the 63.5-cm NTT evaluated here. One advantage of using a larger telescope is that fewer elements are needed to synthesize a given aperture, thus reducing array complexity without

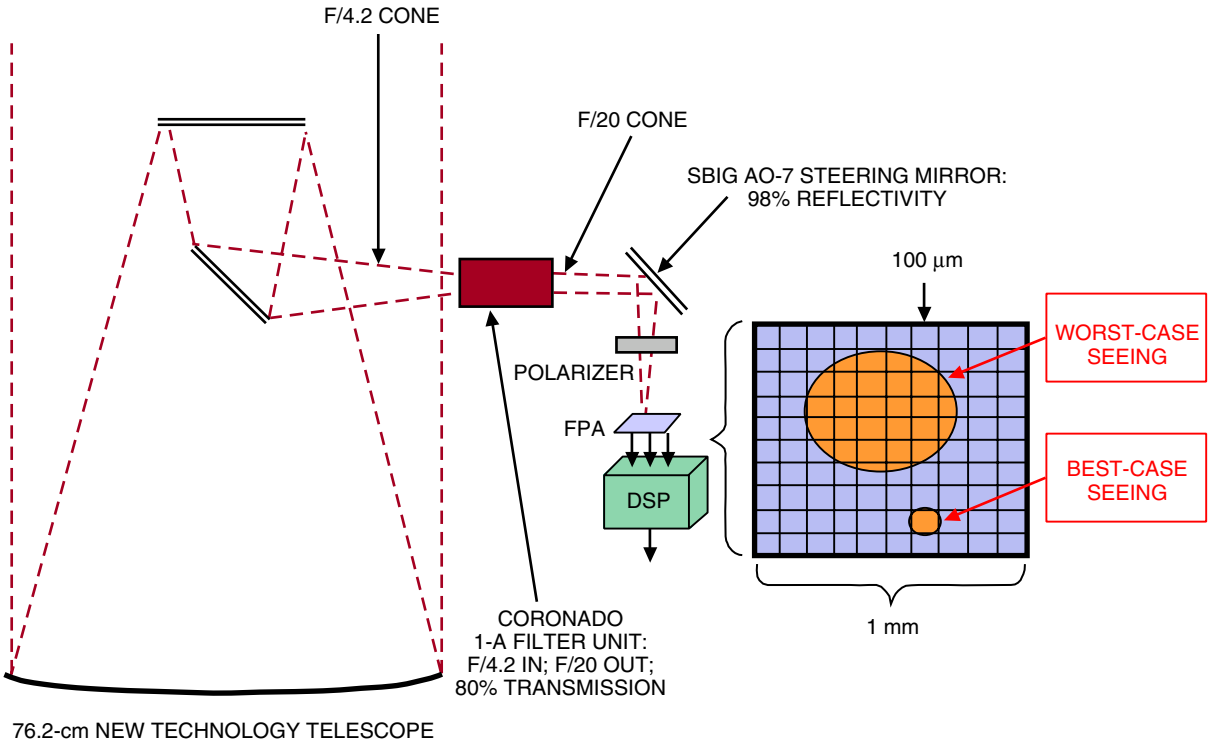

Fig. 2. Optical design of an array telescope element, based on the JMI 76.2-cm NTT specifications.

greatly increasing cost. For example, if the goal were to synthesize a single 5-m-diameter telescope with an array of small telescopes, then we would need $(5/0.762)^2 = 43$ telescopes of 76.2-cm diameter, or $(5/0.635)^2 = 62$ telescopes of 63.5-cm diameter (since area is proportional to the square of the diameter). The cost-complexity trade-off favors the larger telescope for an operational array. However, with nearly identical design and performance, the smaller telescopes are more cost effective to evaluate.

The 76.2-cm NTT is a folded Newtonian design, much like the 63.5-cm NTT, but with a focal-length-to-diameter ratio of 4.2 (or F/4.2) instead of 5. The cone angle of the light from such fast optics first must be collimated before filtering, since narrowband filters of approximately 1-Å bandwidth around 1064 nm (the laser wavelength) require collimated light for proper operation. Commercial units available from manufacturers such as Coronado Instruments in Arizona supply custom-designed filter assemblies that include a collimator at the input, matched to the cone angle of the telescope, and produce an output beam with virtually any desired F ratio. In order to accommodate a commercial fast-steering mirror, such as the AO-7 "adaptive optics" assembly manufactured by the Santa Barbara Instrument Group (SBIG), a slow F ratio of 20 was selected for this conceptual design. The filtered signal light therefore can be steered closed loop using real-time error estimates from the focal-plane detector assembly. The filtered and fine-steered light then passes through a polarizer to reduce background radiation by approximately 3 dB and impinges on the surface of the high-speed photodetector array.

This focal-plane array is envisioned to be a photon-counting Geiger-mode avalanche photodiode detector (GAPD) array with fast detector recovery times, modeled after the 4×4 GAPD arrays manufactured by aPeak, Inc., of Massachusetts, but with extended response in the infrared for efficient operation at 1064 nm. These detector arrays have individually accessible elements, generate a 3-V square pulse of approximately 50-ns duration in response to a detected photon, and, therefore, require no follow-on amplification, and also can be fabricated as 8×8 or even larger arrays. Typically, each detector array is custom-fitted with a matching lenslet array to provide a high fill factor (94 percent typically). The illustration in Fig. 2 is a 10×10 array, with 100-μm pitch, and approximately 1 mm on a side.

The electrical pulses generated by the GAPD array, each representing a detected photon, are processed by the FPA signal processing assembly, which assembles the detected photons into a sample stream suitable for transmission to the array processor (or transmits them in a different format but without loss of information) and generates local pointing updates for the fast-steering mirror, thus keeping the signal distribution centered over the array despite turbulence and other rapid disturbances. It also monitors slowly evolving phenomena, such as drift due to imperfect telescope alignment or predict residuals, and supplies suitable updates to the telescope drive assembly. Extreme cases of near-perfect seeing, representing little or no turbulence, as well as worst-case seeing are illustrated in Fig. 2. To account for worst-case seeing, the FOV of the telescope and array together must be great enough to encompass the largest average point-spread function in the focal plane, nominally as great as 50 μrad or about 10 arcsec.

A detailed block diagram of the signal-processing functions necessary for arraying direct-detected optical signals is shown in Fig. 3. Electrical pulses from each $N \times N$ focal-plane detector array are processed in the FPA electronics card of each telescope to determine the total number of detected photons per sample time and to extract local information, such as pointing updates and instantaneous point-spread function (PSF) estimates, to further reject background photons via adaptive focal-plane processing, as described in [2]. Samples from each telescope then are assembled to facilitate transfer to a central array combiner assembly, which compensates the sample stream from each telescope for delay variations before combining and, thus, maximizing the signal energy in each pulse as well as minimizing the pulse widths. After combining the delay-compensated samples, the array combiner assembly transmits a single sample stream with optimized pulse energies to the digital receiver, which then proceeds to synchronize the combined digital pulses with the received optical pulses, and continuously adjusts the total delay to track out residual Doppler not accounted for by the Doppler predicts. The array combiner assembly also may receive a synchronized pulse position modulation (PPM) reference clock from the receiver, along with symbol decisions and other side information that could be useful to the array, and distributes these references to the array as needed.

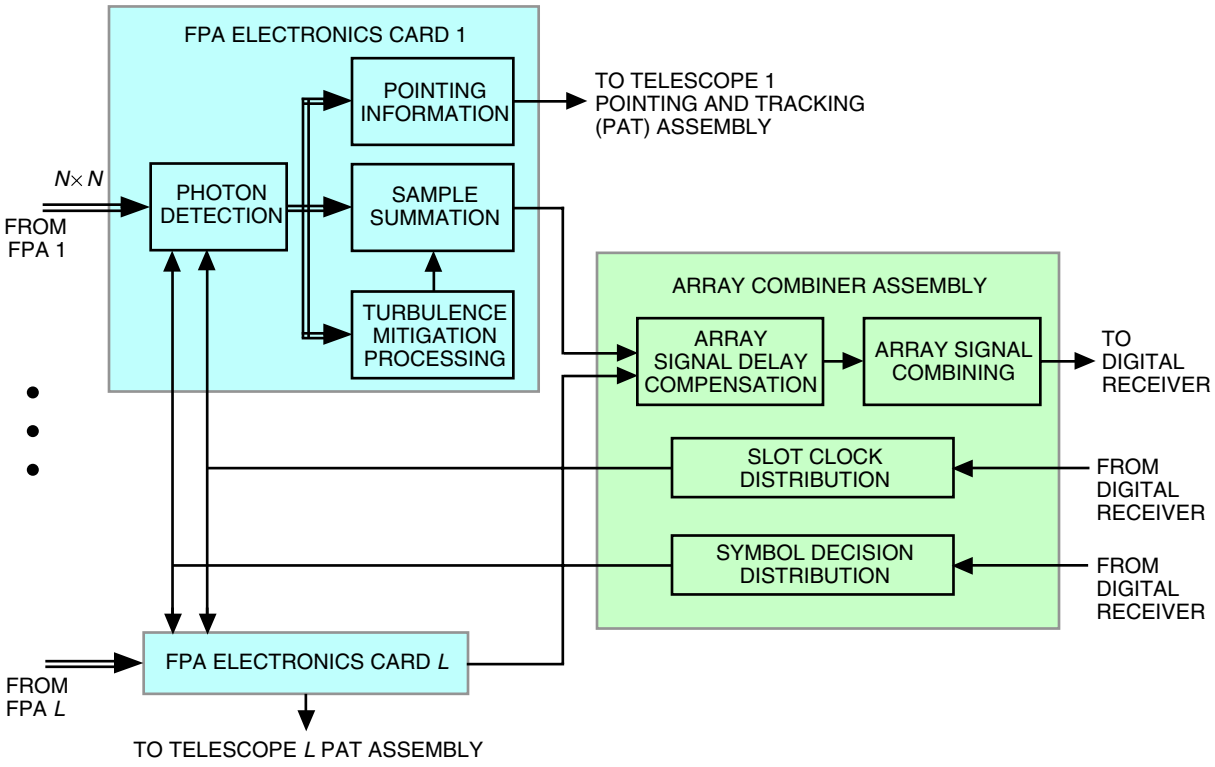

Fig. 3. Block diagram of the signal-processing functions performed by the optical array receiver.

III. Experimental Evaluation of the New Technology Telescope

As described in the previous sections, array detection of the optical signal occurs at a large number of telescopes near-simultaneously, instead of simultaneously as with a single-telescope receiver. This means that the optical array receiver must perform additional processing in order to reconstruct the dispersed photon-detection events occurring over a large number of telescopes. The processing functions are both local and global, meaning that each telescope of the array must play its individual role in the process, but there also must be global coordination to ensure that the local information is interpreted correctly.

As the first elements in the optical detection process, the array telescopes are required to perform predict-driven source acquisition, followed by accurate closed-loop tracking to maximize the received signal power. The experiments performed during the summer and fall of 2003 on the JPL Mesa Antenna Range were aimed at evaluating the blind pointing and closed-loop tracking capabilities of a candidate array telescope. After examining several options, a 63.5-cm New Technology Telescope (NTT) manufactured by Jim's Mobile, Inc. (JMI) of Colorado was selected. This telescope is mounted on a computer-driven altitude–azimuth (or "alt-az") mount, and has sufficient aperture and built-in calibration functions to qualify it as a viable element of a future optical array. It is functionally the same as larger telescopes built by the same manufacturer. Cost was also a major consideration in this choice, especially since the demonstration of arraying capabilities requires the purchase of another telescope of the same design.

The telescope was set up on the JPL Mesa Antenna Range and calibrated using its built-in calibration functions. Initial calibration consists of first pointing the telescope approximately west in a horizontal position, recording the encoder readings, and then invoking either two-point or three-point alignment. This is implemented by selecting suitable stars visible at the time of the experiment, entering their coordinates into the telescope's computer from the database (equivalent to source predicts in an operational scenario), and then commanding the telescope to point towards the selected star. Based on the simple

initial information provided by the encoder readings when pointing due west, the gears are driven to the new coordinates, but inadvertently miss their target by as much as several degrees. The target then is acquired visually through the finder or through an eyepiece, and the telescope is driven to the true coordinates; this correction then is entered into the computer. Next, another star is selected from the database, its coordinates entered into the computer, and the process repeated, usually with much better results. After correcting any residual errors visually, the two-point alignment process is complete; the computer learned the orientation of its own axes with respect to the celestial coordinates. If not for errors in the gears, structural imperfections, and elevation-dependent sag of the telescope itself, this alignment procedure could be made accurate enough for most blind-pointing applications. However, by repeating the alignment process one more time, three-point alignment theoretically could be obtained, which would also account for the telescope distortions. However, three-point calibration was found to be difficult in practice and was achieved only on two occasions over the summer. When sufficient time and effort were devoted to succeed with three-point alignment, the results were rewarding: after three-point alignment, stars in the vicinity of the alignment targets usually could be acquired very accurately on the first try. A 30-mm eyepiece with a 50-deg apparent FOV was used, yielding approximately 100 power with the 63.5-cm F/5 system; this means the true FOV of the eyepiece is approximately 1/2 deg. After three-point alignment, new stars typically were found in the center half of the eyepiece, representing approximately 250-mdeg blind-pointing accuracy.

As previously described, a large-aperture but relatively inexpensive commercially available telescope was selected and procured for evaluation purposes. The telescope is a 63.5-cm-diameter folded Newtonian design, with a focal length of 3.18 m (the photograph in Fig. 1). In addition to the telescope, a real-time computer-driven tip–tilt mirror assembly designated as the AO-7 Adaptive Optics Accessory was purchased from the Santa Barbara Instrument Group (SBIG), along with a customized charge-coupled device (CCD) imaging, tracking, and data-acquisition assembly, designated the Star Tracker Video (STV). Closed-loop tracking and various other functions were tested using the STV CCD camera auto-tracking system, together with the SBIG AO-7 tip–tilt mirror assembly, shown in Fig. 4.

The CCD camera together with the STV were used to simulate the high-speed GAPD array and the closed-loop tracking functions provided by the signal processing assembly. The system was configured to derive pointing corrections from the image of the point source on the CCD camera (stars were used exclusively in these experiments) and to either drive the telescope gears directly or activate the tip–tilt mirror assembly to remove pointing errors introduced by drive-gear imperfections, wind, and image motion due to turbulence.

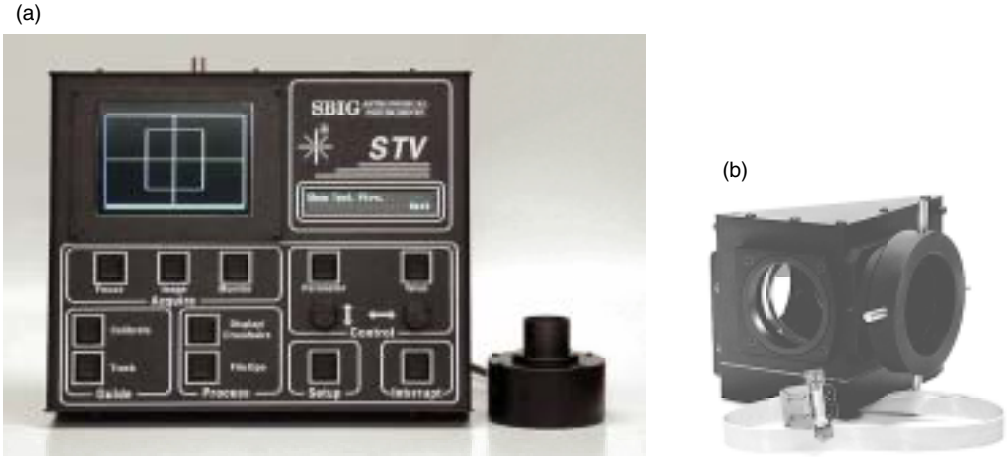

Fig. 4. The SBIG (a) STV CCD camera auto-tracking system and (b) AO-7 tip—tilt mirror assembly.

Figures 5(a) and 5(b) show "snapshot" images of the 2.1-magnitude star Nunki in Sagittarius taken a few seconds apart with the CCD imaging camera on September 3, 2003, under good seeing conditions. These snapshots reflect the effects of turbulence on the PSF in the focal plane and typically change on the order of milliseconds. A commercially available narrowband filter was used for these experiments, with a bandwidth of 8 nm centered at the hydrogen beta wavelength of 486 nm.

At this wavelength, the full-width diffraction-limited field of view of this telescope is approximately $(2.44 \times 0.486\ \mu\text{m}/0.635\ \text{m}) = 1.87\ \mu\text{rad}$; at an effective focal length of 3.18 m, this gives rise to a point-spread function of approximately 6 μm in diameter. The pixels in the imaging camera are 7.4 μm across; therefore, a diffraction-limited star image should occupy only a single pixel under perfect conditions. However, under actual operating conditions, the images are seen to be approximately 10 to 15 pixels across, with numerous "hot spots" that reflect the random concentration of signal energy into different spatial modes on time scales of 10 to 100 ms. These experimentally obtained focal-plane intensity distributions are seen to be very similar to the simulated distributions used in the simulations described in [1], validating the use of phase screens together with Fourier transformation, as described in [1,2]. Figure 5(c) shows a real-time estimate of the average half-power angle of the star image, along with a three-dimensional rendering of the instantaneous intensity distribution. Half-power angles typically were 2 arcsec under good seeing conditions, consistent with the size of the turbulence-degraded star images shown in Figs. 5(a) and 5(b).

The tracking performance of the 63.5-cm NTT was evaluated on four separate occasions on the JPL Mesa Antenna Range, all under average seeing conditions. Representative tracking data are shown in Figs. 6(a) and 6(b), where closed-loop tracking of the star Nunki was recorded on September 10. Figure 6(a) shows the azimuth and elevation corrections applied directly to the drive gears of the telescope as a function of time, derived from the motion of the star image over the CCD array. In this mode, large corrections typically were required to overcome backlash and other imperfections in the gears. Figure 6(b) shows the response of the AO-7 tip–tilt mirror assembly: when large gear errors or light wind gusts were encountered, large corrections were applied in a single direction in order to keep the image centered over the CCD array, as shown in the central part of the track in Fig. 6(b) and to a lesser extent in Fig. 6(a).

The graphs in Fig. 7 show closed-loop tracking of the star Schedar (α Cassiopeia) under good conditions using both the telescope drive gears and the AO-7 tip–tilt mirror assembly. The corrections were applied separately to the telescope gears and to the AO-7 mirror, because the commercial test equipment did not have simultaneous tracking capability. It can be seen that, under good tracking conditions, only small corrections need to be applied to keep the star centered, as shown in Fig. 7(a). When the tracking was

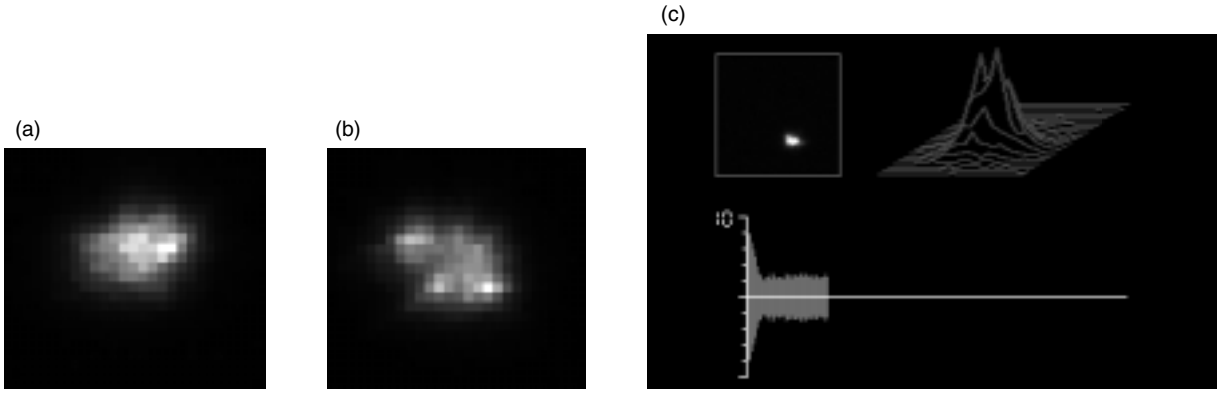

Fig. 5. Point-spread function: (a) a real-time image of the star Nunki, showing degradation of the PSF due to turbulence, (b) the same as (a), taken a fraction of a second later, and (c) a real-time estimate of PSF diameter and a three-dimensional rendering of instantaneous intensity of the star Schedar (α Cassiopeia).

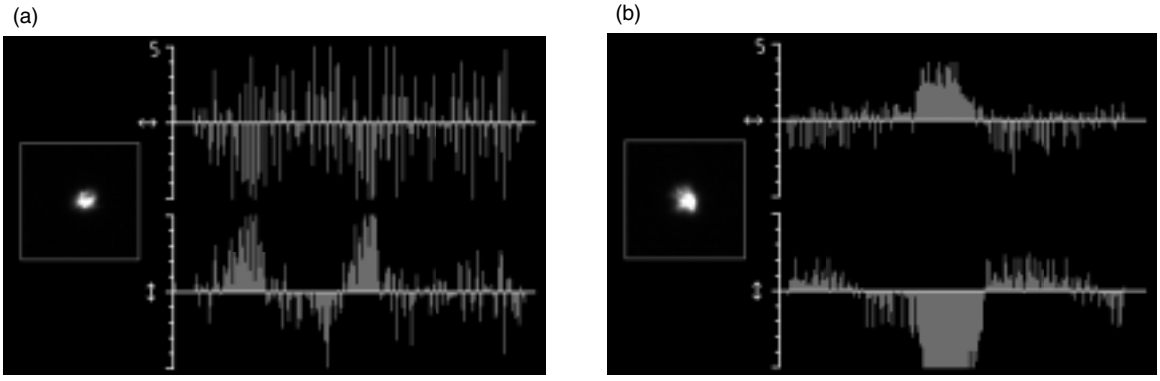

Fig. 6. Real-time tracking errors applied to (a) the telescope drive gears and (b) the AO-7 tip—tilt mirror to keep Nunki centered over the array. Despite the large offsets near the center of the track in (b) to overcome wind effects, the star image remained centered in the tracking subarray.

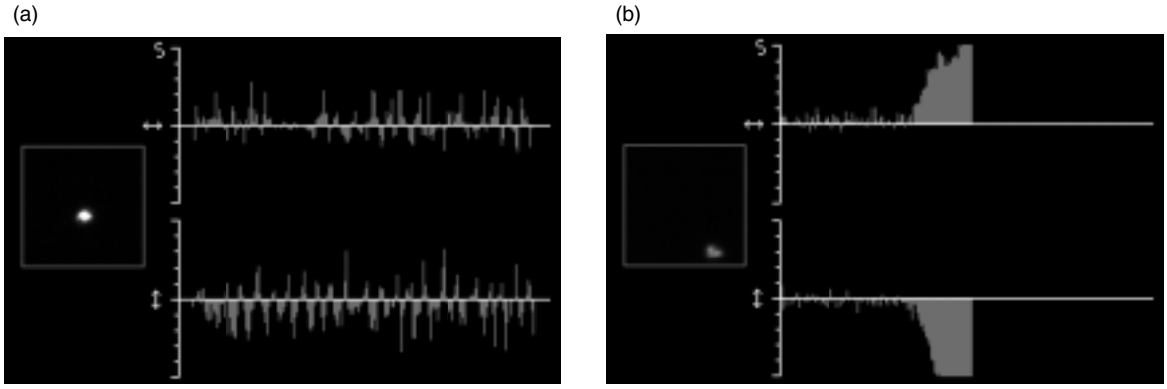

Fig. 7. Closed-loop tracking of the star Schedar (α Cassiopeia): (a) real-time tracking errors applied to the telescope drive gears under good conditions (no wind) and (b) corrections applied to the AO-7 mirror assembly, showing the effects of the untracked drift component.

switched to the AO-7 mirror assembly, only small updates were required at first, as can be seen in Fig. 7(b); however, uncompensated drift components along both pointing coordinates resulted in accumulated drift that eventually exceeded the range of the AO-7 mirror. When this occurred, the pointing errors increased dramatically, and the star eventually drifted off center. This example illustrates the importance of removing both the slowly varying drift components, typically resulting from misalignment and predict residuals, and the rapidly varying disturbances caused by turbulence and wind.

With the commercial equipment used for these evaluation experiments, these tracking modes could be applied separately only, but in an operational system these two modes would operate simultaneously to correct and fine-tune telescope pointing and keep the signal distribution centered over a small photon-counting detector array. Closed-loop tracking therefore appears to be a viable technique for fine-pointing the individual telescopes of an optical array receiver autonomously, based only on local measurements once the source has been acquired by the tracking system.

IV. Conclusions

Large-aperture telescopes are difficult to construct and maintain, require massive support structures and drive assemblies, and represent a single point of failure. In addition, once constructed, the collecting area of a single telescope cannot be easily expanded to meet demands for enhanced performance in future missions. An array of small telescopes, on the other hand, provides a robust, scalable, parallel receiver architecture that easily expands to accommodate greater demands. The concept of an optical array receiver suitable for deep-space communications has been defined in a previous article, where the theoretical foundations of optical array receiver operation and performance also were established [1]. The performance of optical array receivers was shown to be equivalent to the performance of the large single-aperture receiver, thus demonstrating that array performance matches single-aperture performance under operating conditions of interest.

In this article, the previously developed theoretical concepts were extended to practical considerations of array implementation. A functional block diagram of the optical array receiver was developed and a conceptual design of the optical components of an array element presented. Preliminary calibration, tracking, and data-gathering experiments conducted on the JPL Mesa Antenna Range were described. It was found that all of the functional capabilities needed for array operation can be found in commercially available telescopes today, although not necessarily in the form required for this application. These capabilities include predict-driven pointing, autotrack, and measurement of local parameters necessary for optimizing array performance. Based on the concept presented in this article and the preliminary test conducted using a commercial off-the-shelf telescope, we concluded that an array-based optical receiver can be implemented with currently available technology.

References

[1] V. Vilnrotter, C.-W. Lau, M. Srinivasan, R. Mukai, and K. Andrews, "An Optical Array Receiver for Deep-Space Communications through Atmospheric Turbulence," *The Interplanetary Network Progress Report 42-154, April–June 2003*, Jet Propulsion Laboratory, Pasadena, California, pp. 1–21, August 15, 2003. http://ipnpr.jpl.nasa.gov/tmo/progress_report/42-154/154I.pdf

[2] V. Vilnrotter and M. Srinivasan, "Adaptive Detector Arrays for Optical Communications Receivers," *IEEE Transactions on Communications*, vol. 50, no. 7, July 2002.